PAPER

Screen-printing of flexible semi-transparent electrodes and devices based on silver nanowire networks

To cite this article: K Elen *et al* 2018 *Nanotechnology* **29** 425201

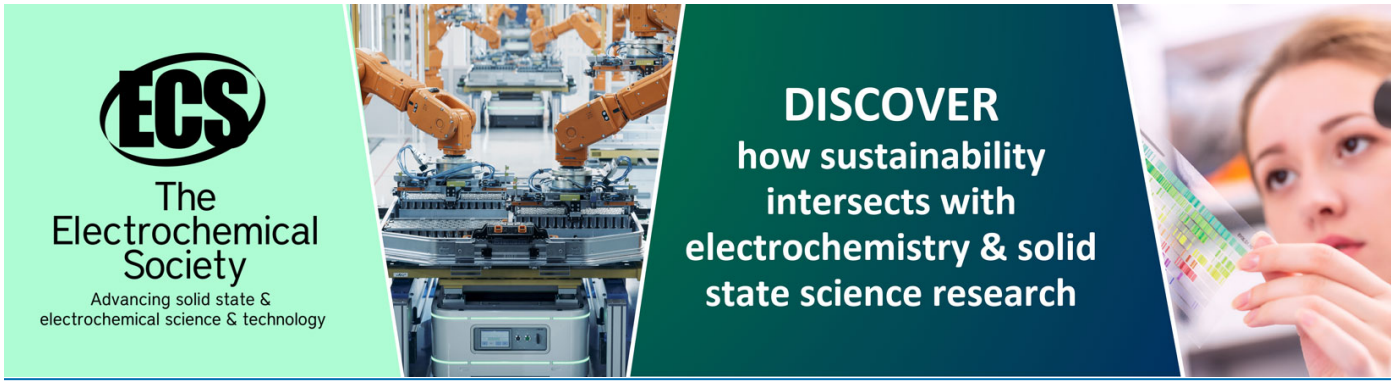

IOP Publishing Nanotechnology
Nanotechnology 29 (2018) 425201 (9pp) https://doi.org/10.1088/1361-6528/aad74d

Screen-printing of flexible semi-transparent electrodes and devices based on silver nanowire networks

K Elen[1,2], H Penxten[3], S Nagels[1,4], W Deferme[1,4], L Lutsen[1], A Hardy[1,2] and M K Van Bael[1,2]

[1] IMEC vzw, IMOMEC Associated Laboratory, Wetenschapspark 1, B-3590 Diepenbeek, Belgium
[2] UHasselt, Institute for Materials Research (IMO), Inorganic and Physical Chemistry, Agoralaan Building D, B-3590 Diepenbeek, Belgium
[3] UHasselt, Institute for Materials Research (IMO), Organic and Bio-Polymer Chemistry, Agoralaan Building D, B-3590 Diepenbeek, Belgium
[4] UHasselt, Institute for Materials Research (IMO), Functional Materials Engineering, Wetenschapspark 1, B-3590 Diepenbeek, Belgium

E-mail: marlies.vanbael@uhasselt.be

Received 24 April 2018, revised 28 May 2018
Accepted for publication 31 July 2018
Published 13 August 2018

Abstract

Silver nanowire networks have demonstrated significant potential as semi-transparent electrodes for various applications. However, for their widespread utilisation in devices, upscaled coating technologies such as screen-printing need to be explored and related to this, the formulation of suitable inks is indispensable. This work contributes to this effort by the synthesis of Ag-NW based formulations. The rheological characteristics that are essential for screen-printing are obtained by the addition of hydrophobically modified cellulose. The electrical and optical characteristics of screen-printed features on PET are compared by a Van der Pauw method and UV–vis spectroscopy. Despite the presence of the cellulose additive, the screen-printed electrodes exhibit a transmittance from 92.8% to 57.3% and a sheet resistance down to 27 Ohm sq^{-1}. Based on the percolation theory in composites, a mathematical expression is presented, which allows the in-depth analysis of the resulting opto-electrical properties. The application potential of the nanowire-containing formulations is finally demonstrated by screen-printing functional, flexible electroluminescent devices.

Supplementary material for this article is available online

Keywords: metallic nanowires, transparent conductive coating, ink formulation, printed electronics, screen-printing, low temperature, modelling

(Some figures may appear in colour only in the online journal)

Introduction

Semi-transparent electrodes are an essential component in many optoelectronic devices, such as touch screens, flat panel displays and photovoltaic cells [1]. Currently, semi-transparent conductive oxides (TCOs)—notably indium tin oxide (ITO)—are the prevailing materials that are used in this context [2]. Nonetheless, metal nanowire networks seem a promising concept for replacing ITO as the semi-transparent electrode in a range of applications [3, 4]. In such networks, the nanowires conduct charge carriers, while the open areas allow the transmission of light. Furthermore, nanowire-based electrodes possess assets that are generally not achievable for TCOs. They are for example flexible [4–6], stretchable [7, 8], printable and exhibit a performance equivalent to ITO upon thermal processing at moderate temperatures (below 150 °C) [3], which make them ideal for printing semi-transparent conductive features on plastic substrates. The combination of these qualities

has invoked significant research interest towards the synthesis and application of metallic nanowires. Silver nanowires [8–18] attract most attention, but also copper [19–24] and cupronickel [25] demonstrate promising results. One of the first methods for the reproducible synthesis of silver nanowires was reported by Sun and Xia [14, 15]. In their 'polyol method' silver nitrate and polyvinyl pyrrolidone (PVP) are dissolved in ethylene glycol. Upon heating the silver is reduced by the glycol, while the PVP acts as a capping agent to ensure a predominant one-dimensional growth of the metallic nanoparticles. Since then, numerous other synthesis recipes for metallic nanowires have been published. A comprehensive review of these recipes can be found in the work of Xiang *et al* [16].

To fabricate semi-transparent conductive coatings from metal nanowire dispersions several coating methods are described in literature, such as drop casting [5, 26, 27], spin coating [28–30] or bar coating [6, 31, 32]. In a recent literature review [33], Wu provides an extensive overview of methods and inorganic materials for printed electronics. Compared to conventional lab-scale deposition methods, screen-printing presents a number of advantages towards upscaling, including low cost, few wastes and printing speeds of 5 to 20 m min^{-1} for flat-bed screen-printers up to 150 m min^{-1} using rotary screen-printers [34]. Additionally, screen-printing offers the ability to print the electrodes directly into a predefined pattern, without the need for a subsequent etching step. Screen-printing pastes are however complex formulations that require a specific rheological behaviour. Initially, they must exhibit a high viscosity to avoid material flowing through the openings of the screen before the printing step. During printing the viscosity should decrease, allowing the ink to pass through the mesh. Once on the substrate, the ink should gradually regain its high initial viscosity to avoid spreading out and to retain a clear edge demarcation, yet still allowing levelling of the printed film [34]. Recently, Liang *et al* [7] reported a method for screen-printing non-semi-transparent electrodes using silver nanowires. However, printing pastes for semi-transparent electrodes must meet additional challenging requirements. First of all, the solid loading of nanowires should be considerably lower to ensure a high optical transparency of the printed features. This signifies that the characteristic rheological behaviour of the printing paste should mainly come from additional polymeric species that are included in the formulation. To this end, Hoeng *et al* [35] propose using cellulose nanofibrils for screen-printing semi-transparent Ag-NW electrodes, however, a concentration of 3–8 wt% hydroxypropyl methyl cellulose was still required for optimising the visco-elastic behaviour of the printing pastes. Since these polymeric components will inhibit the transport of electrons across the final nanowire network, their concentration should be kept at a minimum. In other words, to screen-print semi-transparent electrodes an intricate balance between transparency, conductivity and visco-elastic properties must be found. Nevertheless, to our knowledge, a detailed investigation of the combined optical and electrical characteristics of screen-printed Ag-NW networks is yet to be presented.

In this study we compare formulations containing silver nanowires, in which the polymeric component consists of PEDOT:PSS on one hand and cetyl hydroxyethyl cellulose on the other. The introduction of hydrophobic side-chains to the cellulose backbone allows us to minimise the required concentration of the polymer binder in the screen-print formulations. Furthermore, a mathematical model, based on the percolation theory in composites, is amended to correlate the opto-electrical characteristics to the structural properties of the screen-printed NW-networks. Finally, we demonstrate that the optimised formulations can be used successfully in the field of printed electronics by fabricating an AC-powered powder-based electroluminescent (ACPEL) device by means of screen-printing.

Experimental section

Materials

Silver nanowires (Ag-NWs), dispersed in isopropanol, were purchased from Sigma Aldrich and ACS Materials. Clevios™ S V4 was purchased from Heraeus GmbH. Cetyl hydroxyethyl cellulose (CHEC) was provided by Ashland Inc. under the form of Natrosol™ Plus 330 PA. Isopropanol (IPA, anhydrous, >99%) was purchased from Sigma Aldrich.

Ink formulation

Clevios™ S V4, which is supplied as a ready-to-use paste for screen-printing PEDOT:PSS, was used without additional purification. Ag-NWs (dispersed in isopropanol) were added to the paste in order to obtain formulations comprising 0–1 wt% Ag-NWs, 80–100 wt% Clevios and 0–20 wt% isopropanol.

Cetyl hydroxyethyl cellulose (Natrosol™ Plus 330) was supplied as a dry powder and was used without additional purification. Appropriate amounts of the CHEC were first dissolved in deionized water (milliQ, resistivity 18.0 MOhm cm) and stirred at room temperature for at least 24 h to ensure complete solvation. Ag-NWs (dispersed in isopropanol) were then added to obtain formulations comprising 0–1 wt% Ag-NWs, 0–2 wt% CHEC, 58%–98% water and 0–39 wt% isopropanol.

Screen-printing of semi-transparent electrodes

Test features (25 mm × 25 mm) were screen-printed on PET substrates (Melinex 125) using an ISIMAT 1000 semi-automatic screen-printing device. Prior to printing, the PET substrates were cleaned using technical isopropanol and acetone. The printing pastes were loaded onto a monofilament polyester screen mesh (77 threads per cm, 55 μm thread thickness) placed horizontally over the substrate. The Serilor SR1 squeegee (35 mm height, 7 mm width, Shore hardness 75 A) formed an angle of 68° with the screen mesh and the metal flood bar was placed at an angle of 23° with the screen mesh. The printing speed was set to 34 mm s^{-1}. Finally, the printed features were dried at room temperature for 10 min, followed by a heat treatment in a box oven at 120 °C for 10 min to evaporate the remaining solvents.

Device fabrication

The electroluminescent devices in this work consist of a rear silver electrode/insulating layer/phosphor layer/Ag-NW semi-transparent electrode, screen-printed on a PET substrate using an ISIMAT 1000 semi-automatic screen-printing device. All printed components of the ACPEL device were patterned onto a mono-filament polyester screen mesh (77 threads per cm, 55 μm thread thickness). First an Ag paste (Gwent C2131014D3) was screen-printed on PET as the rear electrode for the device, and dried in a box oven at 120 °C for 10 min. Subsequently, the dielectric layer (Gwent D2090130D5) was printed over the Ag rear electrode followed by an intermediate heat treatment at 120 °C for 10 min. The phosphor layer, consisting of Gwent C2080211D2, was screen-printed on top of the dielectric layer and again dried at 120 °C for 10 min. The luminescent area of the ACPEL devices was kept at 55 mm × 55 mm. Finally, the Ag-NW paste was screen-printed on top of the phosphor followed by a final heat treatment at 120 °C for 10 min.

Characterisation

The rheological behaviour of the formulated inks was analysed using an AR-G2 Magnetic Bearing Rheometer (TA Instruments). All measurements were carried out at room temperature. Steady-state flow step tests were performed to measure the shear viscosity of the inks at shear rates of 1–500 s^{-1} . The data from the steady-state flow step test were afterwards analysed using a Cross flow model. To simulate the screen-printing process peak hold step tests were performed with constant shear rates in multiple intervals: first a low shear rate (0,1 s^{-1} for 120 s), followed by a high shear rate (100, 200, 300, 400 or 500 s^{-1} for 30 s) each time followed by an interval at low shear rate (0,1 s^{-1} for 120 s). Stress sweep step tests were performed with an oscillation stress of 0,1 to 100 Pa at a frequency of 1 Hz. The microstructure of the semi-transparent electrodes was visualised by scanning electron microscopy (SEM, Hitachi TM3000). The sheet resistance of the printed electrodes was determined by a Van der Pauw method using a four-point contact measurement. To this end, silver contacts were first placed at the corners of a 25 mm × 25 mm square feature. The transparency of the printed electrodes was recorded in the wavelength range from 300 to 800 nm on an Agilent Cary 5000 UV–vis-NIR spectrophotometer.

Results and discussion

Rheology of the formulated inks

To meet the rheological requirements for screen-printing, two classes of printing pastes were formulated and evaluated: pastes containing PEDOT:PSS on one hand and modified cellulose as the organic binder on the other. The materials that are used in the formulation of the inks are presented in table 1 together with their respective concentration window. Clevios™ S V4 is a ready-to-use formulation for screen-printing PEDOT:PSS.

Table 1. Composition of the formulations for rheology measurements.

Code	Composition
CV	Clevios (100%)
CVAg	Clevios (80%) + Ag-NWs (0,5%) + IPA (19,5%)
NS-0,5	Natrosol (0,5%) + H_2O (99,5%)
NS-1	Natrosol (1%) + H_2O (99%)
NS-2	Natrosol (2%) + H_2O (98%)
NSAg	Natrosol (2%) + H_2O (78%) + Ag-NWs (0,5%) + IPA (19,5%)

Natrosol™ Plus 330 PA is a commercial grade of modified hydroxyethyl cellulose, based on a degree of cetyl hydrophobes grafted onto a hydroxyethyl cellulose backbone.

The Cross flow model [36] was used to fit the data from the steady-state rheology measurements. This procedure provides the critical rheological characteristics of pseudoplastic formulations (table 2). The zero shear viscosity describes the magnitude of the viscosity at the lower range of the Newtonian plateau and is valuable for assessing the thickening effect of the polymers, while the infinite shear viscosity measures the flow behaviour in high shear situations (e.g. during screen-printing). The rate index describes the dependence of the viscosity on the shear rate and is a measure for shear thinning. A value close zero illustrates Newtonian behaviour. The reciprocal of the consistency provides the critical shear rate for the onset of shear thinning. Finally, the thixotropy describes the time dependent response of the viscosity to a change in shear rate and is evaluated by measuring the area enclosed between the two curves in a hysteresis loop.

The results in table 2 clearly show that both Clevios-based pastes have a high (zero shear) viscosity that is suitable for screen-printing. Regarding the Natrosol-based inks only the formulations containing 2% Natrosol (NS-2 and NS-Ag) have a sufficiently high viscosity at high shear rate. Shear thinning is found in all formulations by comparing the zero shear viscosity to the infinite shear viscosity. This pseudoplastic behaviour is further characterised by a rate index between 0,69 and 1,13. The consistency of the Clevios-based pastes is noticeably higher than the cellulose-based inks. Nonetheless, in all pastes shear thinning can be observed at shear rates that are characteristic for screen-printing (100–500 s^{-1}). This can be visualised in the peak hold step tests that mimic the shear conditions during screen-printing (figure 1). Here, the initial viscosity of the formulations, at a low shear rate of 0,1 s^{-1}, is close to the zero shear viscosity, which was obtained from the Cross analysis of the steady-state rheology measurements. During a high shear interval the viscosity decreases to values below 1 Pa s, confirming the pseudoplastic behaviour of the investigated formulations. No major difference in shear thinning is observed for the five high shear rate intervals. The thixotropy of the formulations ensures that at least 90% of the initial viscosity is recovered within 50 s after a high shear step. Maestro *et al* [37] ascribe this thixotropic behaviour of CHEC to a restoration of hydrophobic interactions, which requires a

Table 2. Rheological characteristics of the examined formulations.

	Zero shear viscosity (Pa s)	Infinite shear viscosity (Pa s)	Rate index	Consistency (s)	Normalised thixotropy (s^{-1})
CV	1,82 10^{5}	4,11 10^{-1}	0,69	3,32 10^{5}	1,84 10^{-5}
CVAg	8,40 10^{4}	8,93 10^{-2}	0,72	2,20 10^{5}	3,89 10^{-5}
NS-0,5	4,18 10^{-2}	6,83 10^{-3}	1,06	7,23 10^{-3}	2,54 10^{-5}
NS-1	5,63 10^{-1}	2,45 10^{-2}	1,13	2,79 10^{-2}	1,51 10^{-5}
NS-2	8,15 10^{0}	3,94 10^{-2}	0,81	2,26 10^{-1}	1,55 10^{-5}
NSAg	1,29 10^{1}	3,05 10^{-2}	0,76	3,55 10^{-1}	2,39 10^{-5}

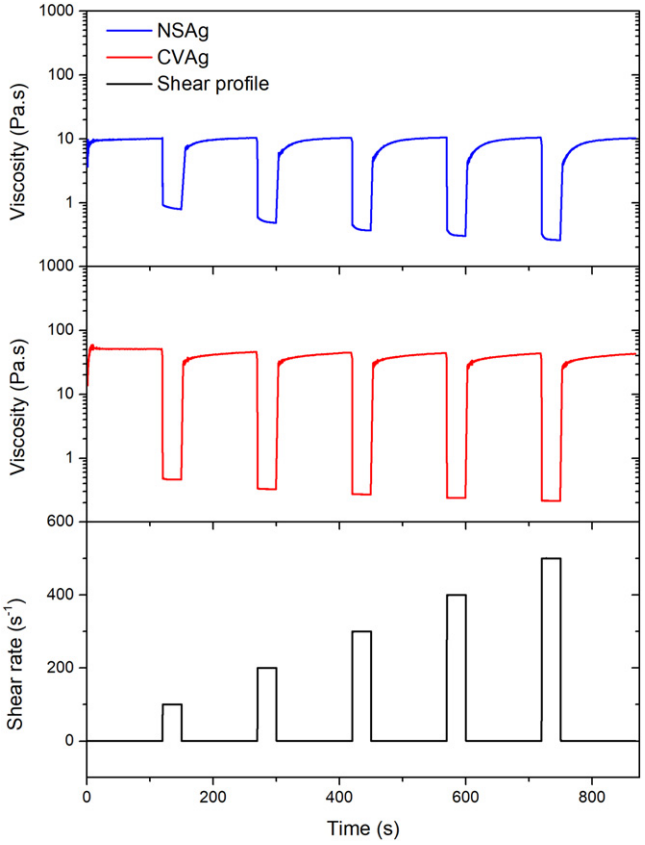

Figure 1. Peak hold step tests on Clevios(CV)-based and cellulose (NS)-based formulations containing Ag-NWs, mimicking the shear conditions during screen-printing.

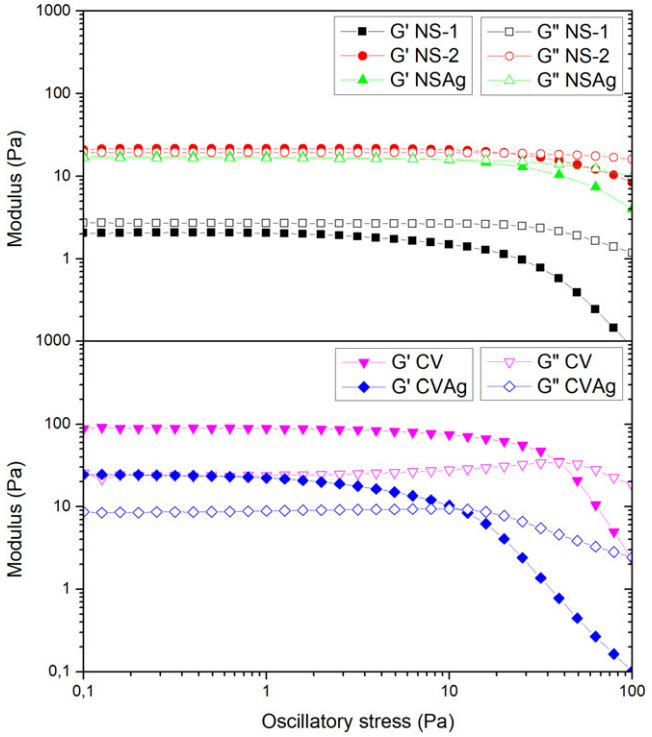

Figure 2. Effect of the oscillatory stress on the storage modulus G' and the loss modulus G'' of the Clevios-based and cellulose-based formulations, as determined by stress sweep measurements.

diffusion controlled migration of the cetyl groups through the medium.

The storage modulus (G') and the loss modulus (G'') of the formulations were determined by stress sweep measurements (figure 2). These measurements show that the response of these visco-elastic moduli is primarily determined by the concentration of the polymeric component in the respective formulations. This indicates that they arise through inter- and intramolecular forces between the polymeric chains. At low shear stress, the visco-elastic moduli are minimally affected by the applied stress, demonstrating that the intermolecular forces between the polymeric species are sustained in this stress range. Further increase of the stress leads to a gradual decrease of the moduli. The observation that G' decreases faster than G'' reveals that intermolecular forces are being eliminated and that the paste experiences a transition from a gel-like consistency to a liquid state. This transition is more pronounced in the Clevios-based pastes, where the formulations start with an elastic-dominated behaviour ($G' > G''$) which converts to a viscous-dominated behaviour ($G' < G''$) at a high shear stress.

Opto-electrical properties of the printed features

Based on the results from the rheology measurements, new formulations were prepared for screen-printing test features on PET substrates (table 3). Additional rheology measurements for assessing the rheology of the screen-printed formulations are provided as supplementary material (figure S1 is available online at stacks.iop.org/NANO/29/425201/mmedia). After printing and drying, the printed features have a good adherence to the PET substrate, as demonstrated by a tape test (figure S2), and present a clear edge demarcation. The current work did not target screen-printing of high resolution features and the formulations or print settings were not optimised accordingly. Nonetheless, the NSAg-1,0 formulation was used successfully to

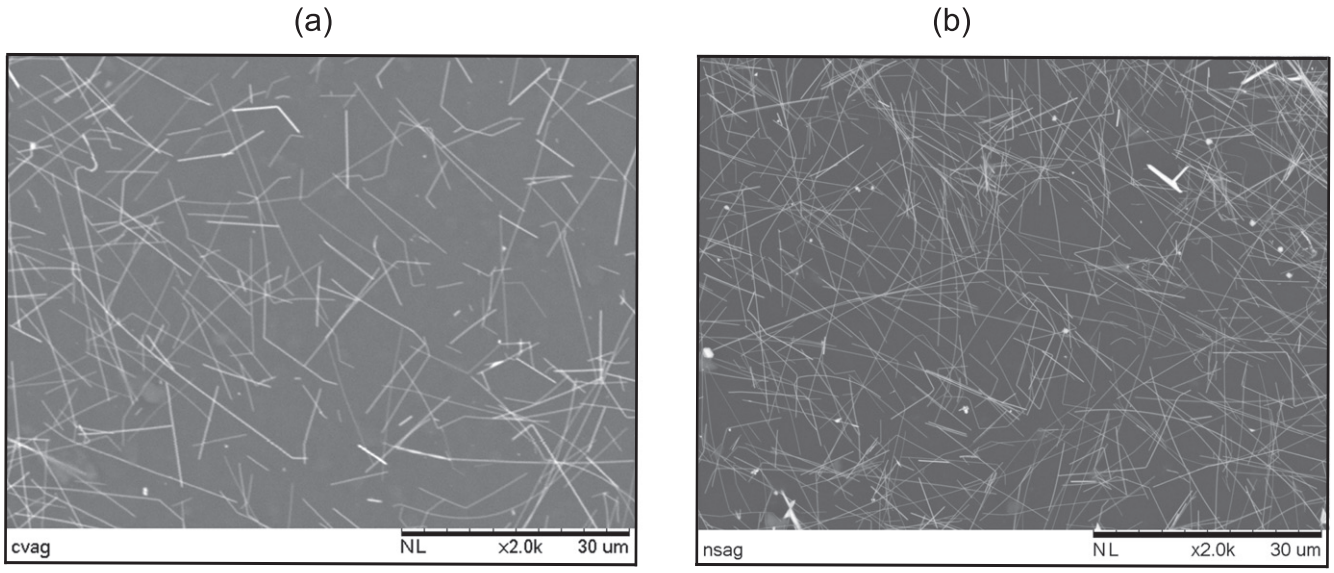

Figure 3. Scanning electron micrographs of features that were printed using a Clevios-based and cellulose-based Ag-NW formulation (a) CVAg-0,5 (b) NSAg-0,5.

Table 3. Composition of the formulations for screen-printing.

Code	Composition
CV	Clevios (100%)
CVAg-0,5	Clevios (80%) + Ag-NWs (0,5%) + IPA (19,5%)
NS	Natrosol (1,5%) + H_2O (78,5%) + IPA (20%)
NSAg-0,25	Natrosol (1,5%) + H_2O (88,5%) + Ag-NWs (0,25%) + IPA (9,75%)
NSAg-0,5	Natrosol (1,5%) + H_2O (78,5%) + Ag-NWs (0,5%) + IPA (19,5%)
NSAg-0,75	Natrosol (1,5%) + H_2O (70,5%) + Ag-NWs (0,75%) + IPA (27,3%)
NSAg-0,9	Natrosol (1,5%) + H_2O (62,5%) + Ag-NWs (0,9%) + IPA (35,1%)
NSAg-1,0	Natrosol (1,5%) + H_2O (58,5%) + Ag-NWs (1%) + IPA (39%)

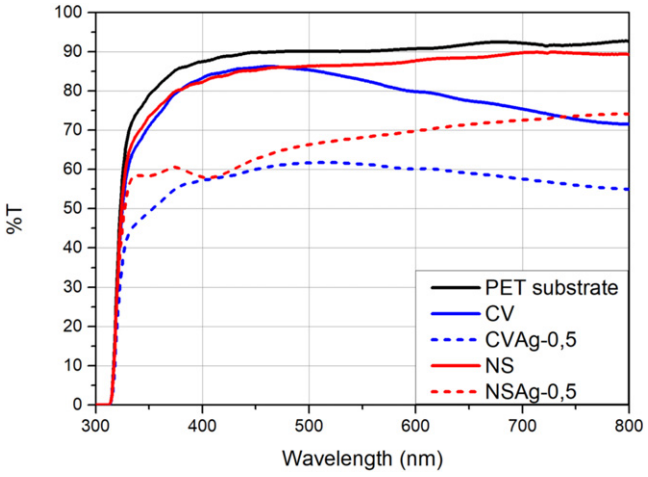

Figure 4. UV–vis-spectra of features that were printed using a Clevios-based and cellulose-based formulation with and without addition of 0,5 wt% of Ag nanowires.

print both lines of ca. 400 μm and features separated at a distance of ca. 400 μm. Corresponding optical micrographs are included as supplementary material (figure S3). SEM micrographs of the printed features demonstrate a random distribution of the Ag-NWs throughout the polymer matrix (figure 3), creating a network that will facilitate the transport of electrons.

Features that were printed using a Clevios-based formulation exhibit a blue colour, based on visual inspection, whereas the cellulose-based formulations render quasi-colourless features. Clevios-based formulations contain PEDOT:PSS, which is known to absorb light in the red and infra-red region. This becomes clearly visible by comparing the UV–vis spectra of features that were printed using Clevios-based and cellulose-based formulations (figure 4). The introduction of nanowires to all formulations leads to a general reduction in transparency. In contrast to the Clevios-based pastes, where light absorption of the organic component is significant, we find that the transparency of the features that are printed using a cellulose-based paste is primarily determined by the concentration and dimensions of the Ag-NWs in the formulation. Here, the transmission of light T through a film with thickness t, containing a volume fraction Φ_{NW} of nanowires, can be described by the Beer–Lambert Law:

$$A = -\log(T) = \alpha\, \Phi_{NW}\, t. \quad (1)$$

This equation shows a linear correlation between the attenuance (A)—a quantity describing the decrease in transparency by a combination of absorption, reflection and scattering—

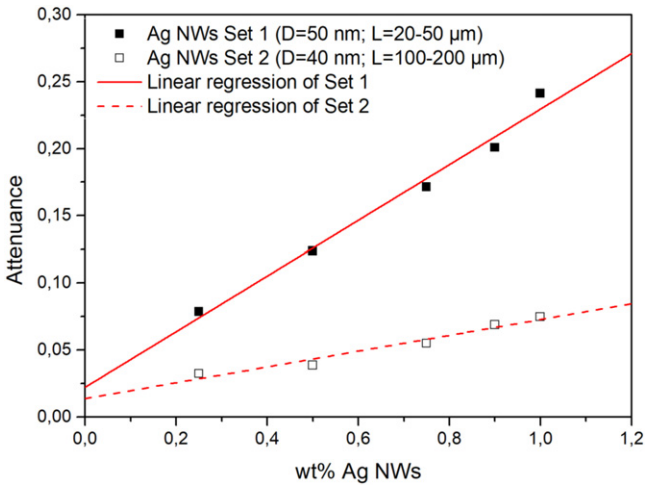

Figure 5. Demonstration of a linear correlation between the concentration of Ag-NWs in the formulation and the attenuance of the printed features.

and the volume fraction (Φ_{NW}) of nanowires, which is determined by the attenuation coefficient (α) corresponding to that volume fraction. In addition, the volume fraction is proportional to the weight fraction (X_{NW}) of Ag-NWs in the ink formulation through:

$$\Phi_{NW} = \frac{X_{NW}(\delta_m/\delta_{NW})}{(1 - X_{NW})(1 - \delta_m/\delta_{NW})}. \quad (2)$$

Here, δ_m/δ_{NW} describes the ratio of densities of the organic matrix to the silver. By applying the Beer–Lambert law to the experimental data for the printed electrodes, we indeed observe a linear correlation (figure 5). This graph also demonstrates that the attenuation coefficient—which corresponds to the slope of the linear regression—depends on the dimensions of the Ag-NWs that are included in the ink formulation. In fact, the longer NWs in this study (Set 2) appear to have a lower attenuation coefficient. This observation demonstrates that the transparency of the printed electrodes will be less affected by the concentration of Ag-NWs in the ink when longer nanowires are used for its formulation. The intercept of the linear regressions in figure 5 corresponds to a minimal amount of light absorption by the cellulose binder.

By the addition of Ag-NWs to a Clevios-based formulation, the sheet resistance of the printed features can be decreased from 181 to 38 Ohm sq^{-1}, indicating that a nanowire network improves the conductivity. A similar observation can be made for cellulose-based formulations. In this case the sheet resistance can be decreased to 27 Ohm sq^{-1} after the addition of Ag-NWs. The conductivity in composites is determined by the percolation theory, which describes a power law dependence of the conductivity (σ) to the volume fraction (Φ_{NW}) of a conductive filler material in an insulating matrix, when the percolation threshold ($\Phi_{NW,p}$) is approached

$$\sigma = \sigma_0(\Phi_{NW} - \Phi_{NW,p})^k. \quad (3)$$

In this equation, σ_0 is a coefficient that mainly depends on the conductivity of the nanowires and their contact resistance. The exponent (k) is determined by the structure and connectivity of the network. By combining this equation with the Beer–Lambert law and taking into account that the product of the thickness (t) and the sheet resistance (R_s) of the electrode is inversely proportional to the conductivity, following expression is obtained:

$$\frac{1}{R_s} = \frac{\sigma_0}{\alpha^k\, t^{k-1}}(A - A_p)^k. \quad (4)$$

For TCOs, Gordon *et al* [38] described an inverse relation between the sheet resistance and the attenuance and suggested to use the correlation coefficient σ/α as a figure of merit:

$$\frac{1}{R_s} = \frac{\sigma}{\alpha}A. \quad (5)$$

The attentive reader may notice the mathematical similarity between the Gordon expression and equation (4). In fact, the Gordon expression appears to be a special form of equation (4), where the threshold attenuance (A_p) equals zero and the exponent equals one. This is reasonable, since Gordon describes the opto-electrical properties of a uniform and homogeneous layer, whereas equation (4) also applies to conductive networks, embedded in an insulating matrix, as is the case for screen-printed nanowire networks.

Since both the sheet resistance and the attenuation can be measured directly on the semi-transparent electrodes, equation (4) provides a convenient model for a semi-empirical analysis of the opto-electrical properties of nanowire networks. This is demonstrated in figure 6, where the inverse sheet resistance is plotted versus the attenuation for two sets of screen-printed electrodes, one set composing nanowires with an average diameter of 50 nm and lengths between 20 and 50 μm, and the second set containing nanowires with an average diameter of 40 nm and lengths between 150 and 200 μm. The experimental results are in good agreement with the provided model and subsequent regression analysis, using a Belehradek equation, yields three descriptive parameters for the opto-electrical characteristics, that are summarised in table 4. Features that are printed using Ag-NWs of Set 1 have a superior conductivity as demonstrated by the higher value of parameter a, which is descriptive of the electron transport across the network. This observation is potentially related to the narrow diameter of the nanowires in Set 2, in combination with a relatively high contact resistance, due to the presence of a polymeric binder. Nonetheless, the transparency of Set 2 is higher than for Set 1, which corresponds to the lower percolation threshold and its associated attenuance, described by parameter b. This is in agreement with Monte Carlo simulations, which have shown that the percolation threshold decreases for longer nanowires [23]. Parameter c, finally, corresponding to the exponent k, is for both sets of Ag-NWs close to 2. This parameter depends on the order and dimensionality of the NW-network and is expected to approach a value of 2 for a three-dimensional network [39]. From this analysis we can conclude that longer nanowires are noticeably beneficial for improving the opto-electrical properties. However, further enhancement of the conductivity requires improving the electron transport across the network, which is (partially) inhibited by the polymer component in the printed films.

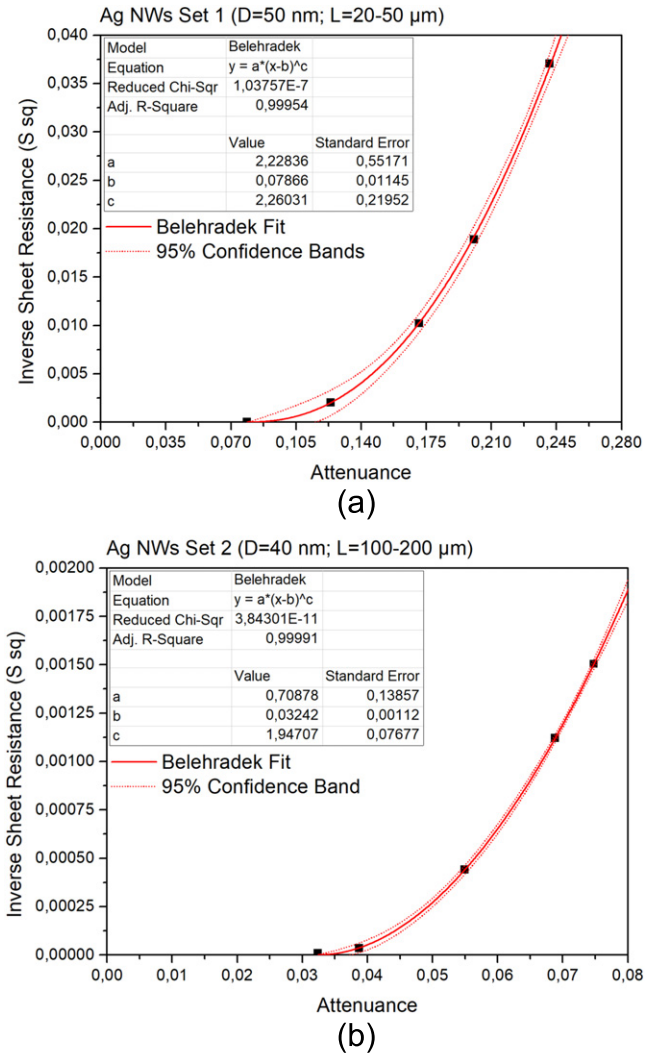

Figure 6. Opto-electrical properties of two sets of nanowire networks and corresponding regression analysis (a) Set 1: $D = 50$ nm; $L = 20$–50 μm (b) Set 2: $D = 40$ nm; $L = 100$–200 μm.

Table 4. Results of the regression analysis of the opto-electrical characteristics of two sets of Ag-NW networks.

Belehradek parameter	Physical definition	Ag-NWs-Set 1 $D = 50$ nm; $L = 20$–50 μm	Ag-NWs-Set 2 $D = 40$ nm; $L = 150$–200 μm
a	$\frac{\sigma_0}{\alpha^k t^{k-1}}$	2,22 ± 0,55	0,71 ± 0,13
b	A_p	0,079 ± 0,012	0,032 ± 0,001
c	k	2,26 ± 0,22	1,95 ± 0,08

The mechanical stability of the printed electrodes on PET is evaluated by a cyclic bending test consisting of 100 cycles of bending around a stylus with a diameter of 1,2 cm. The sheet resistance was recorded periodically after 10 consecutive bending cycles. After completion of 100 cycles, no visible defects, such as cracks, are observed and the electrodes exhibit a stable electric performance with a minor increase of sheet resistance by no more than 5% (figure S4). Its property to tolerate mechanical bending can be attributed to the flexibility of long Ag-NWs and their optimal adherence to the substrate [18].

The screen-printed Ag-NW based (semi-)transparent electrodes, presented here, already have a clear application potential in the field of flexible electronics. To illustrate this, electroluminescent devices were fabricated on PET in which all functional components were deposited by screen-printing. For the deposition of the semi-transparent top electrode the 'NSAg-1,0' formulation was used that demonstrated a transmittance of 84,2% and a sheet resistance of 665 Ohm sq^{-1}, resulting in the optimal balance between transparency and conductivity according to the Haacke figure of Merit. ACPEL devices rely on the emission of light by a phosphor when it is subjected to a strong electrical field [40, 41]. To prevent the formation of short-circuits through imperfections in the phosphor layer an insulating layer is included between the rear electrode and the phosphor. Figure 7(a) shows a schematic cross section of the device, indicating the various components that were used for the fabrication of the ACPEL devices. The phosphor layer can be activated by applying an AC-signal (80 V, 400 Hz) between the rear and semi-transparent electrode. A photograph of a flexed, luminous ACPEL device is presented in figure 7(b) and to illustrate that the device remains operational during repeated bending cycles, a short animation is also provided as electronic supplementary material.

Conclusions

Silver nanowire inks were formulated in view of depositing semi–semi-transparent electrodes by screen-printing. Distinctive attention is directed to ensuring that these formulations fulfil the required rheological specifications, such as a high initial viscosity, shear thinning, and thixotropy. A Cross analysis of the steady-state rheology measurements demonstrated the pseudoplastic behaviour of highly viscous formulations that contain polymeric additives. Their shear thinning and thixotropy was confirmed by peak hold step tests that mimic the shear conditions during screen-printing. The visco-elastic moduli show that the rheology is primarily determined by inter- and intramolecular forces between the polymeric chains. By introducing Ag-NWs to a PEDOT-based formulation, the sheet resistance of the printed features can be decreased to values below 40 Ohm sq^{-1}, indicating that a nanowire network improves the conductivity of the printed electrodes. However, these PEDOT-based features appear blue due to undesirable absorption of red and infra-red light. Colourless features are obtained after screen-printing cellulose-based formulations, characterised by a transmittance from 92,8% to 57,3% at 550 nm and a sheet resistance down to 27 Ohm sq^{-1}. The opto-electrical properties of these nanowire networks are analysed in detail by a semi-empirical model, based on the percolation theory in composites. Here we find that the electron transport is inhibited to some extent by the polymer binder, yet the percolation threshold can be decreased by use of longer nanowires. Finally, the nanowire-based electrodes were successfully implemented in a flexible

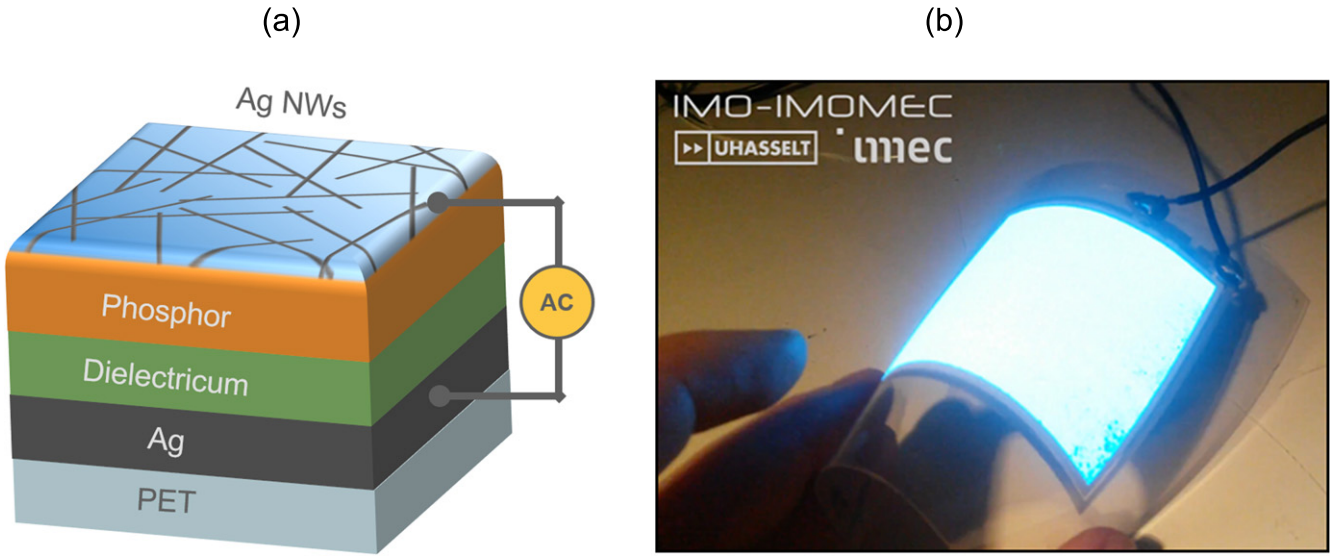

Figure 7. (a) Schematic cross section of the printed electroluminescent device and (b) photograph of a flexed, luminous ACPEL device.

electroluminescent device on PET. These results demonstrate that the presented formulations are a promising approach towards the fabrication of printed optoelectronic components.

Acknowledgments

This project has received funding from the European Union's Horizon 2020 research and innovation programme under grant agreement No. 641864. The authors would like to acknowledge Dr Pieter Samyn (UHasselt) for providing the SEM micrographs.

ORCID iDs

K Elen https://orcid.org/0000-0001-6907-0355

References

[1] Kulkarni G U, Kiruthika S, Gupta R and Rao K D M 2015 Towards low cost materials and methods for transparent electrodes *Curr. Opin. Chem. Eng.* **8** 60
[2] Pasquarelli R M, Ginley D S and O'Hayre R 2011 Solution processing of transparent conductors: from flask to film *Chem. Soc. Rev.* **40** 5406
[3] Ye S R, Rathmell A R, Chen Z F, Stewart I E and Wiley B J 2014 Metal nanowire networks: the next generation of transparent conductors *Adv. Mater.* **26** 6670
[4] Langley D, Giusti G, Mayousse C, Celle C, Bellet D and Simonato J P 2013 Flexible transparent conductive materials based on silver nanowire networks: a review *Nanotechnology* **24** 452001
[5] Yu Z B, Zhang Q W, Li L, Chen Q, Niu X F, Liu J and Pei Q B 2011 Highly flexible silver nanowire electrodes for shape-memory polymer light-emitting diodes *Adv. Mater.* **23** 664
[6] Liu C H and Yu X 2011 Silver nanowire-based transparent, flexible, and conductive thin film *Nanoscale Res. Lett.* **6** 8
[7] Liang J, Tong K and Pei Q 2016 A water-based silver-nanowire screen-print ink for the fabrication of stretchable conductors and wearable thin-film transistors *Adv. Mater.* **28** 5986
[8] Xu F and Zhu Y 2012 Highly conductive and stretchable silver nanowire conductors *Adv. Mater.* **24** 5117
[9] Coskun S, Aksoy B and Unalan H E 2011 Polyol synthesis of silver nanowires: an extensive parametric study *Cryst. Growth Des.* **11** 4963
[10] Gottesman R, Tangy A, Oussadon I and Zitoun D 2012 Silver nanowires and nanoparticles from a millifluidic reactor: application to metal assisted silicon etching *New J. Chem.* **36** 2456
[11] Huang G W, Xiao H M and Fu S Y 2015 Wearable electronics of silver-nanowire/poly(dimethylsiloxane) nanocomposite for smart clothing *Sci. Rep.* **5** 13971
[12] Johan M R, Aznan N A K, Yee S T, Ho I H, Ooi S W, Singho N D and Aplop F 2014 Synthesis and growth mechanism of silver nanowires through different mediated agents ($CuCl_2$ and NaCl) polyol process *J. Nanomater.* **2014** 105454
[13] Korte K E, Skrabalak S E and Xia Y N 2008 Rapid synthesis of silver nanowires through a CuCl- or $CuCl_2$-mediated polyol process *J. Mater. Chem.* **18** 437
[14] Sun Y G and Xia Y N 2002 Large-scale synthesis of uniform silver nanowires through a soft, self-seeding, polyol process *Adv. Mater.* **14** 833
[15] Sun Y G, Yin Y D, Mayers B T, Herricks T and Xia Y N 2002 Uniform silver nanowires synthesis by reducing $AgNO_3$ with ethylene glycol in the presence of seeds and poly(vinyl pyrrolidone) *Chem. Mater.* **14** 4736
[16] Xiang X Z, Gong W Y, Kuang M S and Wang L 2016 Progress in application and preparation of silver nanowires *Rare Met.* **35** 289
[17] Yao S S and Zhu Y 2014 Wearable multifunctional sensors using printed stretchable conductors made of silver nanowires *Nanoscale* **6** 2345
[18] Xue Q W, Yao W J, Liu J, Tian Q Y, Liu L, Li M X, Lu Q, Peng R and Wu W 2017 Facile synthesis of silver nanowires with different aspect ratios and used as high-performance flexible transparent electrodes *Nanoscale Res. Lett.* **12** 12
[19] Chang Y, Lye M L and Zeng H C 2005 Large-scale synthesis of high-quality ultralong copper nanowires *Langmuir* **21** 3746

[20] Mohl M, Pusztai P, Kukovecz A, Konya Z, Kukkola J, Kordas K, Vajtai R and Ajayan P M 2010 Low-temperature large-scale synthesis and electrical testing of ultralong copper nanowires *Langmuir* **26** 16496
[21] Nam V B and Lee D 2016 Copper nanowires and their applications for flexible, transparent conducting films: a review *Nanomaterials* **6** 17
[22] Ye S R, Rathmell A R, Stewart I E, Ha Y C, Wilson A R, Chen Z F and Wiley B J 2014 A rapid synthesis of high aspect ratio copper nanowires for high-performance transparent conducting films *Chem. Commun.* **50** 2562
[23] Ye S R, Stewart I E, Chen Z F, Li B, Rathmell A R and Wiley B J 2016 How copper nanowires grow and how to control their properties *Acc. Chem. Res.* **49** 442
[24] Yin Z, Lee C, Cho S, Yoo J, Piao Y and Kim Y S 2014 Facile synthesis of oxidation-resistant copper nanowires toward solution-processable, flexible, foldable, and free-standing electrodes *Small* **10** 5047
[25] Rathmell A R, Nguyen M, Chi M F and Wiley B J 2012 Synthesis of oxidation-resistant cupronickel nanowires for transparent conducting nanowire networks *Nano Lett.* **12** 3193
[26] Lee J Y, Connor S T, Cui Y and Peumans P 2008 Solution-processed metal nanowire mesh transparent electrodes *Nano Lett.* **8** 689
[27] Lee J Y, Connor S T, Cui Y and Peumans P 2010 Semitransparent organic photovoltaic cells with laminated top electrode *Nano Lett.* **10** 1276
[28] Chung C H, Song T B, Bob B, Zhu R, Duan H S and Yang Y 2012 Silver nanowire composite window layers for fully solution-deposited thin-film photovoltaic devices *Adv. Mater.* **24** 5499
[29] Chung C H, Song T B, Bob B, Zhu R and Yang Y 2012 Solution-processed flexible transparent conductors composed of silver nanowire networks embedded in indium tin oxide nanoparticle matrices *Nano Res.* **5** 805
[30] Leem D S, Edwards A, Faist M, Nelson J, Bradley D D C and de Mello J C 2011 Efficient organic solar cells with solution-processed silver nanowire electrodes *Adv. Mater.* **23** 4371
[31] Hu M J, Gao J F, Dong Y C, Li K, Shan G C, Yang S L and Li R K Y 2012 Flexible transparent PES/silver nanowires/PET sandwich-structured film for high-efficiency electromagnetic interference shielding *Langmuir* **28** 7101
[32] Ye S R, Rathmell A R, Ha Y C, Wilson A R and Wiley B J 2014 The role of cuprous oxide seeds in the one-pot and seeded syntheses of copper nanowires *Small* **10** 1771
[33] Wu W 2017 Inorganic nanomaterials for printed electronics: a review *Nanoscale* **9** 7342
[34] Faddoul R, Reverdy-Bruas N and Blayo A 2012 Formulation and screen printing of water based conductive flake silver pastes onto green ceramic tapes for electronic applications *Mater. Sci. Eng.* B **177** 1053
[35] Hoeng F, Denneulin A, Reverdy-Bruas N, Krosnicki G and Bras J 2017 Rheology of cellulose nanofibrils/silver nanowires suspension for the production of transparent and conductive electrodes by screen printing *Appl. Surf. Sci.* **394** 160
[36] Cross M M 1965 Rheology of non-newtonian fluids—a new flow equation for pseudoplastic systems *J. Colloid Sci.* **20** 417
[37] Maestro A, Gonzalez C and Gutierrez J M 2002 Shear thinning and thixotropy of HMHEC and HEC water solutions *J. Rheol.* **46** 1445
[38] Gordon R G 2000 Criteria for choosing transparent conductors *MRS Bull.* **25** 52
[39] Mutiso R M 2013 Electrical percolation in metal nanowire networks for bulk polymer nanocomposites and transparent conductors, and resistive switching in metal/polymer nano-gap devices *PhD Thesis* Paper 902 University of Pennsylvania
[40] Deferme W and Verboven I 2018 *Narrow and Smart Textiles* ed Y Kyosev *et al* (Cham: Springer) p 259
[41] Verboven I, Stryckers J, Mecnika V, Vandevenne G, Jose M and Deferme W 2018 Printing smart designs of light emitting devices with maintained textile properties *Materials* **11** 290